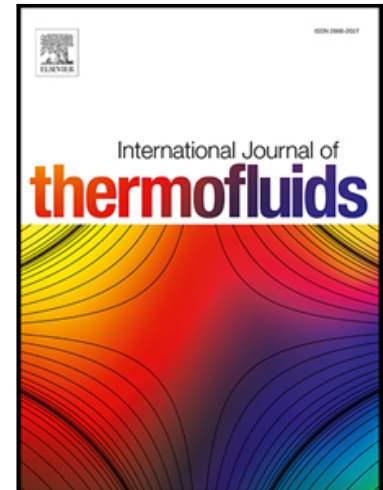# Journal Pre-proof

Mathematical model of a proton-exchange membrane (PEM) fuel cell

Abdelnasir Omran , Alessandro Lucchesi , David Smith ,
Abed Alaswad , Amirpiran Amiri , Tabbi Wilberforce ,
José Ricardo Sodré , A.G. Olabi

Please cite this article as: Abdelnasir Omran , Alessandro Lucchesi , David Smith , Abed Alaswad , Amirpiran Amiri , Tabbi Wilberforce , José Ricardo Sodré , A.G. Olabi , Mathematical model of a proton-exchange membrane (PEM) fuel cell, *International Journal of Thermofluids* (2021), doi: https://doi.org/10.1016/j.ijft.2021.100110

Mathematical model of a proton-exchange membrane (PEM) fuel cell

Abdelnasir Omran[1], Alessandro Lucchesi[2], David Smith[1], Abed Alaswad[1], Amirpiran Amiri[1],

Tabbi Wilberforce[1], José Ricardo Sodré[1], A.G. Olabi[1,3]

1. Mechanical Engineering and Design, School of Engineering and Applied Science, Aston University, Aston Triangle, Birmingham B4 7ET.
2. School of Engineering, University of Pisa, Pisa, Italy.
3. Dept. of Sustainable and Renewable Energy Engineering, University of Sharjah, P.O. Box 27272, Sharjah, United Arab Emirates

ABSTRACT

This work presents a mathematical modelling of a proton-exchange membrane fuel cell (PEMFC) system integrated with a resistive variable load. The model was implemented using *MATLAB Simulink* software, and it was used to calculate the fuel cell electric current and voltage at various steady-state conditions. The electric current was determined by the intersection of its polarisation curve and applied as an input value for the simulation of the PEM fuel cell performance. The model was validated using a *Horizon H-500xp* model fuel cell stack system, with the following main components: a 500 W PEM fuel cell, a 12 V at 12 A battery for the start-up, a super-capacitor bank to supply peak loads and a 48 V DC-DC boost converter. The generated power was dissipated by a variable resistive load. The results from the model shows a qualitative agreement with test bench results, with similar trends for stack current and voltage in response to load and hydrogen flow rate variation. The discrepancies ranged from 2% to 6%, depending on the load resistance applied. A controlled current source was utilised to simulate the variation of fan power consumption with stack temperature, ranging from 36.5 W at 23°C to 52 W at 65°C. Both model and experiments showed an overall PEMFC system maximum efficiency of about 48%.

Keywords: Fuel cell; hydrogen; mathematical model; simulation; energy.

1. INTRODUCTION

As industries from energy and transportation sectors join efforts with governments to find solutions to reduce greenhouse gas (GHG) emissions, hydrogen is seen as one of the most promising alternatives to replace conventional fossil fuels [1 - 7]. Recent progress in hydrogen fuel cell technology can revolutionise the future scenario of transportation vehicles alongside the introduction of electric cars [8 – 20]. Although there are many types of fuel cells, the proton exchange membrane fuel cell (PEMFC) type became a popular choice for vehicular application [21 – 28]. The electrochemical conversion in a PEMFC requires a battery for a start-up, air and hydrogen supply, heat removal, and exhaust. The level of complexity of the reaction and energy interaction between the components and the environment, and the high costs of experimental studies stimulate the development of simulation models [29]. In addition, fuel cell stack optimisation is challenging and control of the many accessories during operation is a difficult task as they affect the system performance and efficiency.

Mathematical modelling of fuel cell systems is a convenient way to reduce research time and costs, while providing in-depth analysis of various parameters that affect fuel cell performance and efficiency such as stack temperature, pressure, reactant moisture and air stoichiometry. A previous study using a one-dimensional mathematical model for a fully hydrated and isothermal PEMFC concluded that the higher the cell current density, the greater the threshold of oxygen or air bleeding [29]. Simulink modelling was successfully used to develop a temperature controller for the cooling system of an urban bus PEMFC stack, keeping the target temperature in the range of ±0.5°C [30]. A bench test study using a mathematical model to simulate the ability of a battery-PEMFC hybrid control system proved its efficiency to manage the energy supply for an electric vehicle [31]. An energy

management system was designed using neural network to control the power flux from the fuel cell and battery of a hybrid vehicle, showing its suitability for real-time vehicle controller [32]. Modelling and simulation of fuel cells has also been used to study fuel-air flow patterns [33] and to perform an exergetic analysis [34].

This work aims to develop a steady-state mathematical modelling of a PEMFC system using MATLAB Simulink and compare it results with experiments in a test bench. The mathematical model simulates the output current, voltage and power of the fuel cell, analysing the response of the system with different external loads. The model is compared using the data from commercial Horizon H-500XP fuel cell stack, which main components are a 500 W PEMFC stack, a 12 VDC battery for the start-up and a bank of super-capacitors to supply additional power. In addition to that, the generated power is dissipated in a variable resistive load, where the voltage is maintained constant by a 48-volt DC-DC boost converter. A controlled current source is used to simulate the variation of fan power consumption with stack temperature, ranging from 36.5 W at 23°C to 52 W at 65°C.

2. MATHEMATICAL MODEL

2.1. Fuel cell stack model

Fuel cells are usually modelled with the current as an independent variable used to calculate the stack voltage. In the presented model, the external load resistance is the independent parameter to influence current and voltage [35]. The fuel cell stack has been modelled with a DC voltage source controlled by equations that relate fuel cell stack current and temperature with its voltage. The stack current flows from the voltage source to the circuit. The voltage source supplies energy to an electrical circuit made by a DC boost converter and variable load. The converter is controlled by a voltage Proportional-Integral (PI) controller with pulse-width modulation (PWM) signal control. The controlled current

source models the power consumption of auxiliary components. The whole model is developed with MATLAB Simulink, including its package Simscape to solve the electrical circuit.

The stack was modelled as unidimensional and isothermal, and steady state operating conditions were assumed. The partial pressure of the reactants was taken as constant, while the rise of pressure due to the blower and pressure drop of the fuel flow in the pipe was neglected. The humidity of the membrane was considered constant at saturated conditions. Power consumption of the auxiliary components was also taken as constant. As the transient conditions during start-up is not taken into account by the model, the battery and super-capacitor are not included. The maximum power demand was considered as 600 W. **Error! Reference source not found.** shows a schematic diagram of the PEMFC system.
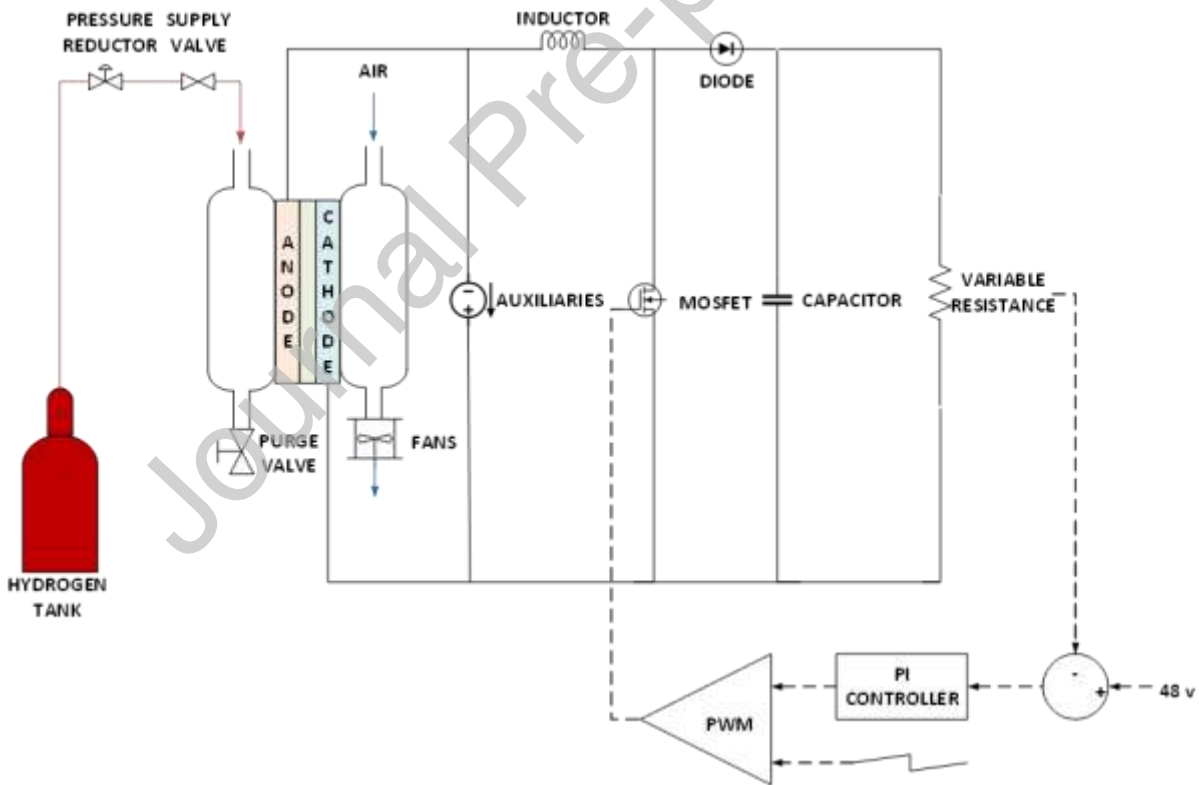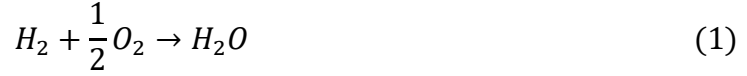

Figure 1. Schematics of PEMFC system.

Hydrogen (H_2) reaction with oxygen (O_2) in a single cell with liquid water (H_2O) as

4

product is written as:

$$H_2 + \frac{1}{2}O_2 \rightarrow H_2O \tag{1}$$

Based on Eq. (1), the reversible open-circuit voltage at the reference condition (298.15 K, 1 bar), E^0, is given by [10]:

$$E^0 = \frac{-\Delta g_f}{2F} = 1.229\ V \tag{2}$$

where Δg_f (kJ/kmol) is the variation in the Gibbs free energy of formation and F is the Faraday constant (96485 C).

Using Nernst's equation, the reversible open-circuit voltage, $E^{T,P}$ (V), can be evaluated at different conditions [10]:

$$E^{T,P} = \frac{-\Delta g_f}{2F} + \frac{RT_s}{2F} ln\left(\frac{p_{H_2} \cdot p_{O_2}^{\frac{1}{2}}}{p_{H_2O}}\right) - \frac{\Delta S}{2F}(T_s - 298.15) \tag{3}$$

where T_s is the stack temperature (K), R is the universal gas constant (8.314 kJ/kmol.K), p is the partial pressure of reactants and products (bar), and ΔS is the entropy variation (kJ/kmol.K).

When load is applied, the external current I_{ext} (A) flows and the voltage drops. During operation, a small amount of hydrogen can diffuse through the membrane from the anode to the cathode, where it reacts without producing current and some electrons may cross through the membranes rather than the external load. Those effects are equivalent and are considered by adding a current loss, I_{loss} (A), to the total fuel cell current, I (A), as shown by:

$$I = I_{ext} + I_{loss} \tag{4}$$

where only I_{ext} can be collected by the external load [36].

The voltage needed to keep the electrochemical reactions in the anode and cathode represents the activation voltage losses, ΔV_{act} (V), which can be calculated as [37]:

$$\Delta V_{act} = \xi_1 + \xi_2 T_s + \xi_3 T_s \, ln\big(C_{O_2}\big) + \xi_4 T_s \, ln(I) \tag{5}$$

where the constant parameters $\xi_1 \ldots \xi_4$ are shown by Tab. 1, and C_{O_2} is the concentration of dissolved oxygen (mol/cm^3) at the liquid interface as defined by Henry's law [38];

$$C_{O_2} = \frac{p_{O_2}}{5.08 \times 10^6 . exp\left(-\frac{498}{T_s}\right)} \tag{6}$$

And the equivalent activation resistance is given by:

$$R_{act} = \frac{n_{cell} \Delta V_{act}}{I} \tag{7}$$

where n_{cell} is the number of cells connected in series. The ohmic voltage losses, ΔV_{ohm} (V), are described by [10]:

$$\Delta V_{ohm} = R_{ion} I + (R_{ele} + R_{con}) I_{ext} \tag{8}$$

where R_{ion} (Ω) is the resistance to the flow of ions in the membrane, R_{ele} (Ω) is the electronic resistance to the flow of electrons in the conductive material, and R_{con} (Ω) is the contact resistance of the electrodes. Only R_{ion} is here considered and, for a Nafion-based membrane, it is given by [39]:

6

$$R_{ion} = \frac{\tau_m r_m}{A} = \frac{\tau_m}{A} \cdot \frac{181{,}6\left(1 + 0{,}03\frac{I}{A} + 0{,}062\left(\frac{T_s}{303}\right)^2 \left(\frac{I}{A}\right)^{2{,}5}\right)}{\left(\lambda_m - 0{,}634 - 3\frac{I}{A}\right) \cdot e^{4{,}18\left(\frac{T_s - 303}{303}\right)}} \tag{9}$$

where τ_m is the membrane thickness (cm^2), σ_m is the ionic conductivity of the membrane (Ω/cm), and A is the single cell active area (cm^2). λ_m is the average water content of the membrane and is a function of the water activity a, both dimensionless [40]:

$$\lambda_m = \begin{cases} 0.043 + 17.81a - 39.85a^2 + 36.0a^3 & for \ 0 < a \le 1 \\ 14 + 1.4(a - 1) & for \ 1 < a \le 3 \end{cases} \tag{10}$$

The membrane of the stack is a composite Nafion/ PTFE (polytetrafluoroethylene) membrane [41] with an active area of 76 cm^2 and a thickness of 25 μm. Concentration voltage losses (ΔV_{con}) are introduced to consider the effect on Nernst voltage and activation voltage losses due to the pressure drop in the gas diffusion layer. These losses occur at the high current caused by reduction in gas concentration at the electrode surface, and are given by [36]:

$$\Delta V_{con} = \left(1 + \frac{1}{\alpha}\right)\frac{RT}{nF}\ln\frac{I_L}{I_L - I} \ [V] \tag{11}$$

The equivalent concentration resistance is given by:

$$R_{con} = \frac{n_{cell}\Delta V_{con}}{I} \tag{12}$$

7

where I_L (A) is the limit current of the electrode, which occurs when the partial pressure of the reactants falls down to zero, and n is the number of electrons involved in the electrode reactions. Anode concentration losses are considered negligible, so n = 4 and I_L is the cathode limit current.

A capacitance in parallel with the activation and concentration resistances simulates the transient effect of the double layer charge. The equivalent double layer capacitance of the stack (C_{dl}) has been calculated starting from a single cell capacitance per area equal to $0.01974 \, F/cm^2$. This leads to a single-cell double-layer capacitance of $1.5 \, F$ and to a stack double layer capacitance of the stack (C_{dl}) equal to $0.05 \, F$. At steady state, the polarisation curve of the fuel cell stack is then described by:

$$
\begin{aligned}
V_{stk}(I) = n_{cell}V_{cell}(I) &= n_{cell}(E - \Delta V_{act} - \Delta V_{ohm} - \Delta V_{con}) \\
&= n_{cell}\Big(E - [\xi_1 + \xi_2 T_s + \xi_3 T_s \ln(C_{O_2}) + \xi_4 T_s \ln(I)] - R_{ion}I \\
&\quad - \Big(1 + \frac{1}{\alpha}\Big)\frac{RT}{4F}\ln\frac{I_L}{I_L - I}\Big)
\end{aligned}
$$

(13)

where the number of cells connected in series, n_{cell}, is 30. The output power of the stack is given by:

$$
P_{stk} = V_{stk}I_{ext}
$$

(14)

Air flows inside the cathode flow channels sucked (blown/pushed) by two axial fans sited at the end of the channels. The pressure drop is negligible, thus the pressure inside the channels is atmospheric (p_{atm}). The oxygen partial pressure inside the cathode flow channels is simply given by:

$$
p_{O_2} = X_{O_2}p_{atm}
$$

(15)

8

The oxygen partial pressure can be found considering the inlet air flow oxygen content, oxygen reacted, produced water and water membrane flow from anode to cathode. Thanks to the strong over stoichiometric use of air, the oxygen molar fraction (X_{O_2}) at steady state is constant and equal to the inlet atmospheric air, 21%. Hydrogen is provided at 1.5 bar, and the flow rate is self-adjusted, function of the pressure difference between the inlet and the anode flow channels. At steady-state operation, inlet hydrogen is equal to the reacted hydrogen and the purge valve is closed, thus no hydrogen is stored nor depleted. The pressure difference (Δp_{H_2}) is only due to the frictional effects in the supply valves and pipeline. No water or air, only pure hydrogen is considered inside the anode flow channels. Thus

$$p_{H_2} = p_{H_2,in} - \Delta p_{H_2} \tag{16}$$

The pressure inside the channels must always be higher than atmospheric pressure. When the purge valve is opened, the gas must flow outside the stack not otherwise. Hydrogen pressure drop can be expressed as a function of the squared hydrogen flow rate, $\dot{V}_{H_2}$:

$$\Delta p_{H_2} = k_f \dot{V}_{H_2}^2 \tag{17}$$

where k_f is equal to 2.22×10^{-3} atm·min^2/nl^2. The atmospheric pressure is assumed to be reached with the highest possible flow rate of the supply system, equal to 15 nl/min.

Error! Reference source not found. shows all parameters considered by the PEMFC model.

Table 1. PEMFC model parameters.

PARAMETER	VALUE	PARAMETER	VALUE	PARAMETER	VALUE
p_{H_2} (atm)	$1.0 \div 1.5$	ξ_1	1.00	τ_m (μm)	25
p_{O_2} (atm)	$\simeq 0.21$	ξ_2	-3.4×10^{-3}	λ_m	7

9

| p_{H_2O} (atm) | 1 | ξ_3 | -7.80×10^{-5} | A (cm^2) | 76 |
| I_{loss} (A) | 0.3 | ξ_4 | 1.85×10^{-4} | $I_{L,c}$ (A) | 47 |

2.2. Boost converter and external load model

The use of a PEM fuel cell in a hybrid system requires a DC boost converter shown in Figure 2. Schematics of a basic DC boost converter is shown by Fig. 2 [42]. The PWM signal commands the opening and closing of a switcher with a fixed switching frequency F_{SW} (Hz). The corresponding period of switching (t_{SW}) is the sum of ON (t_{ON}) and OFF (t_{OFF}) times [43]:

$$t_{SW} = \frac{1}{F_{SW}} = t_{ON} + t_{OFF} \tag{18}$$

The duty cycle (*d*) is defined as the portion of time when the switcher is 'ON state', as [43]:

$$d = \frac{t_{ON}}{t_{ON} + t_{OFF}} \tag{19}$$

Assuming the switcher, the diode, the inductor (L) and the capacitor (C) are ideal, the equations that relate the duty cycle, the converter input voltage (V_I) and current (I_I) and the output voltage (V_O) and current (I_O) are given by [42]:

$$\frac{V_O}{V_I} = \frac{1}{1-d} \tag{20}$$

$$\frac{I_O}{I_I} = 1-d \tag{21}$$

Applying Ohm's law on the external load resistance (R_{ld}), one can obtain [42]:

10

$$R_{ld} = \frac{V_O}{I_O} = \frac{\frac{V_I}{(1-d)}}{I_I(1-d)} \tag{22}$$

The equivalent resistance to the fuel cell is given by [42]:

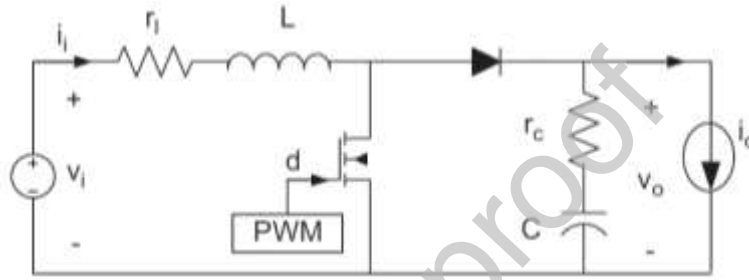$$R_{eq} = \frac{V_I}{I_I} = R_{ld}(1-d)^2 \tag{23}$$

Figure 2. Schematics of a basic DC boost converter circuit.

Equation (23) shows the effect of the duty cycle on the fuel cell operating point, the highest value of duty cycle leads to the lowest equivalent resistances sensed by the fuel cell and, therefore, to the highest current and power demand. The PI controller controls the value of the duty cycle, ensuring 48 V for every external load.

The size of the reactive elements of the boost converter is chosen to limit the input current ripple (fuel cell current ripple) and the output voltage ripple as well. Limiting the fuel cell current ripple is necessary to ensure a longer lifetime of the fuel cell. Sudden changes in the fuel cell current should be limited to avoid starvation problems and degradation of a catalyst layer. This is typically done by controlling the fuel cell current with the boost converter [44]. In this model, a PI voltage controller commands the boost converter to guarantee an output voltage of 48 V, but it does not take into account the fuel cell current variation. **Error! Reference source not found.** shows the maximum current and voltage ripple allowed and the parameters used for the DC boost converter and PI controller.

11

Table 2. DC boost converter and PI controller parameters

DC BOOST CONVERTER	VALUE	PI CONTROLLER	VALUE
Switching frequency (kHz)	50	k_P	0.0001
Maximum input current ripple (%)	4	k_I	0.5
Maximum output voltage ripple (%)	2	Duty cycle range	$0.2 - 0.7$
Inductance (mH)	1.37		
Capacitance (mF)	1.80		

Figure 3 shows the PEMFC equivalent electrical circuit. The fuel cell is modelled with a controlled DC voltage source $V_{stk}(I)$ that is connected to an electric circuit. The value of the stack output current is taken from the circuit and is used to update the value of the stack output voltage. The fuel cell stack is connected to a DC boost converter, which enhances the output voltage of the stack to 48 V at the resistance load bank.
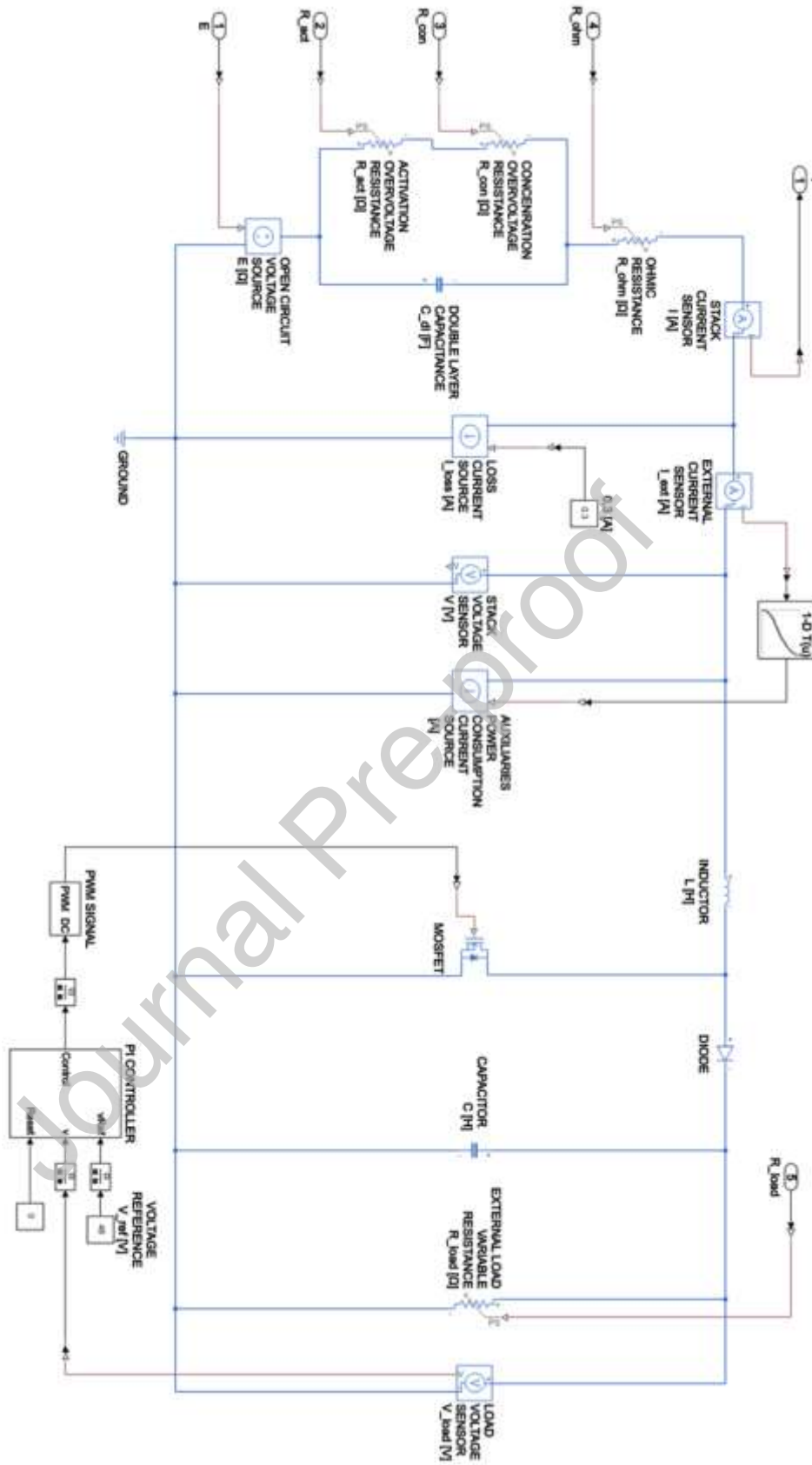
Figure 3. PEMFC system equivalent electrical circuit

A PWM signal, controlled by a PI controller, is used to adjust the duty cycle of the boost converter. After the stack, a controlled current source is used to simulate the power consumption of the auxiliary components, considered variable with stack temperature, ranging from 36.5 W at 296.15 K to 52 W at 338.15 K to take into account the fans power consumption variation with temperature.

2.3. Performance parameters calculation

For a specific external load resistance (R_{ld}), the theoretical power request (P_{ld}) from the stack is calculated by

$$P_{ld} = \frac{V_{ld}^2}{R_{ld}} \tag{24}$$

where V_{ld} is the voltage across the external load (48 V).

The efficiency of the boost converter (η_{con}) is given by its output power (P_{out}) divided by its input power (P_{in}). Therefore, dividing the power delivered to the load (P_{ld}) by the output power of the stack (P_{stk}) minus power consumption by auxiliary components (P_{aux}), the efficiency of the boost converter can be calculated as:

$$\eta_{con} = \frac{P_{out}}{P_{in}} = \frac{P_{ld}}{P_{stk} - P_{aux}} = \frac{\frac{V_{ld}^2}{R_{ld}}}{V_{stk}I_{ext} - P_{aux}} \tag{25}$$

The stack efficiency is calculated by:

$$\eta_{stk} = \frac{P_{stk} - P_{aux}}{P_{H_2}} = \frac{V_{stk}I_{ext} - P_{aux}}{\rho_{H_2}\dot{V}_{H_2}Q_{LHV,H_2}} \tag{26}$$

where P_{H_2} is the power input of hydrogen (W), which is given by the product of its flow rate $\dot{V}_{H_2}$ (m^3/s) multiplied by its density ρ_{H_2} (kg/m^3) and lower heating value Q_{LHV,H_2} (kJ/kg). The

14

number of moles of hydrogen consumed by the stack for the reactions and for losses due to internal fuel crossover, $\dot{N}_{H_2}$ (mol/s), is obtained by [36]:

$$\dot{N}_{H_2} = \frac{n_{cell}I}{2F} \tag{27}$$

The number of moles of hydrogen is essentially equal to the number of moles of fuel because hydrogen with a purity degree of 99.99% has been used. Assuming that the fuel utilisation factor is $\eta_f = 1$ and that hydrogen behaves as an ideal gas, the actual fuel volumetric flow rate, $\dot{V}_{fuel}$ (m^3/s), is calculated as:

$$\dot{V}_{H_2} = \dot{N}_{H_2} \bar{v}_{H_2} \frac{1}{\eta_f} = \dot{N}_{H_2} \frac{\bar{R}T_n}{p_n} \tag{28}$$

where T_n and p_n are respectively the temperature and pressure at the normal condition, 273.15 K and 101.325 kPa, $\bar{v}_{H_2}$ is the fuel specific volume on mole basis (m^3/kmol), and $\bar{R}$ is the universal gas constant (8.314 kJ/kmol.K).

The overall system efficiency η_{sys} is given by the product of the stack efficiency and the DC boost converter efficiency, which becomes:

$$\eta_{sys} = \eta_{stk}\eta_{con} = \frac{P_{ld}}{P_{H_2}} = \frac{\frac{V_{ld}^2}{R_{ld}}}{\rho_{H_2}\dot{V}_{H_2}Q_{LHV,H_2}} \tag{29}$$

3. MATERIALS AND METHOD

3.1. Experimental apparatus

15

The H-500XP model PEM fuel cell stack used in this work has 30 cells with a peak power of 600 W. The current varies from 0 A to 33.5 A, and DC voltage ranges from 15 V to 28.8 V. The rated current is 33.5 A at 18 V. The stack is self-humidified, and is operated with high purity hydrogen (99.99 % dry H_2) and air for the reaction. Cooling is provided by two axial fans. Figure 4 shows the fuel cell system components, including boost converter and external load bank. The main peripheral components are hydrogen cylinder, purging valves and pipe, battery, super-capacitor bank, and system controller.

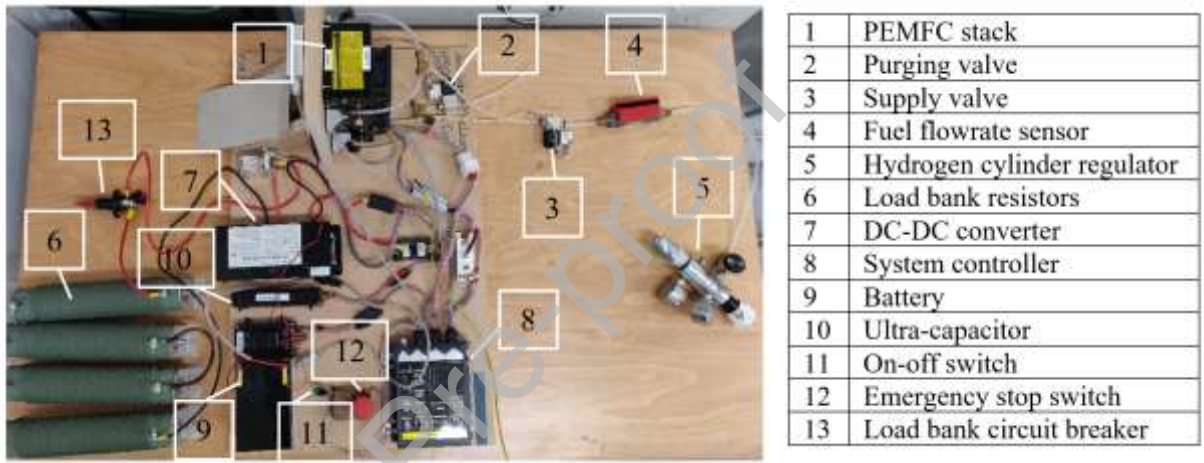| 1 | PEMFC stack |
2	Purging valve
3	Supply valve
4	Fuel flowrate sensor
5	Hydrogen cylinder regulator
6	Load bank resistors
7	DC-DC converter
8	System controller
9	Battery
10	Ultra-capacitor
11	On-off switch
12	Emergency stop switch
13	Load bank circuit breaker

Figure 4. H-500XP and auxiliaries

The fuel cell battery operates for the start-up and the super-capacitor operates supplying power during short circuit to allow for continuous power supply. The controlled system parameters are stack temperature, through variation of the fan velocity, fuel purging valve opening, and fuel supply. The controller also monitors the stack voltage, current and temperature, preventing over-current, low-voltage and high temperature.

The H-500XP stack system is connected to the hydrogen cylinder, DC boost converter, and external resistive loads, which provide variable power demand. The boost converter ensures 48 V across the load system. The power is dissipated to the resistance as heat by the Joule effect. Figure 5 shows the PEMFC system in a purpose-built casing (1), bank of electric resistances (2), and load controller (3). Figure 6 illustrates the complete experimental

16

apparatus, including the added components to ease the functionality and ensure safety operation.
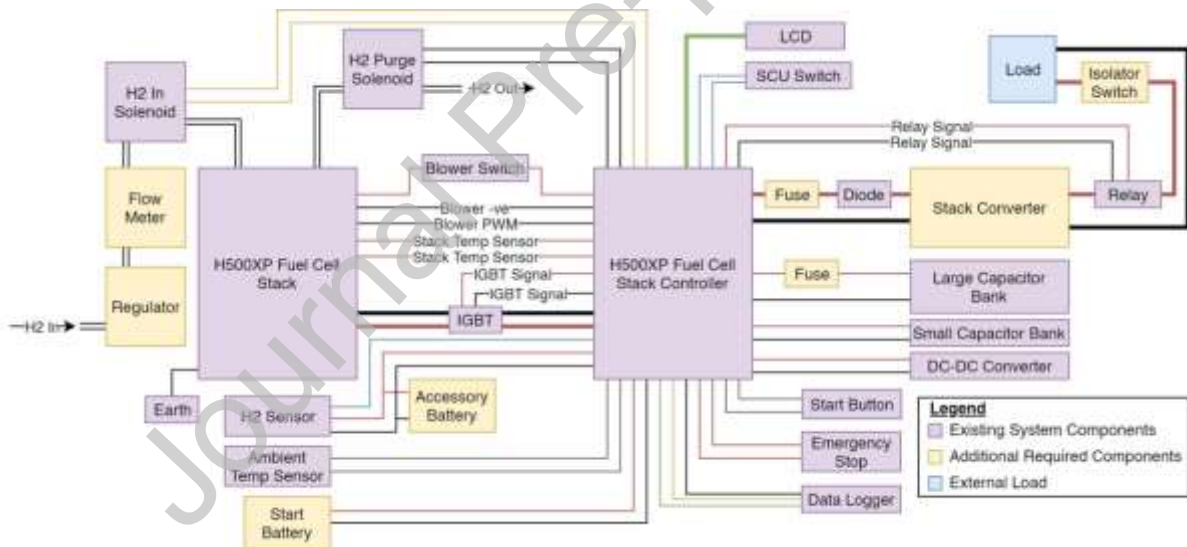

Figure 5. PEMFC test bed.

Figure 6. Schematics of the experimental apparatus.

3.2. Test procedure

The pressure regulator attached to the hydrogen cylinder connected to the PEMFC system was set to supply 1.5 bar absolute. The PEMFC system was monitored using a dedicated software provided by the manufacturer. The battery was used for start-up and then disconnected. The load variation was applied through the load bank control keys. The system was tested with increasing the load, starting from open-circuit condition and gradually reducing to the lowest external load resistance of 4.63 Ω. For every load change, 1 min was allowed to reach the steady-state condition before recording the sensor readings. The readings were recorded along 5 min at a given load. Hydrogen flow rate was recorded by a digital flowmeter positioned between the cylinder and the stack inlet. The instantly acquired data to be processed by the software were: stack voltage (V), stack current (A), stack output power (W), stack temperature (°C), ambient temperature (°C), and battery voltage (V).

4. RESULTS AND DISCUSSION

Figure shows the fuel cell stack polarisation curve, which represents the steady state operating states. The model polarisation curve was fairly close to the experimental values, with a maximum discrepancy of 3.1%. The lowest external load resistance tested was 4.63 Ω, corresponding to the maximum electric current of 29.2 A at 19.67 V, thus providing 574.4 W. Similar comparison of the polarisation curve has been applied elsewhere to certify that the model adequately follows the fuel cell characteristics [45 – 47]. The polarisation curve is sometimes preferred to be represented in terms of electric current density per unit area (A/cm^2) instead of electric current (A) [31, 48, 49].
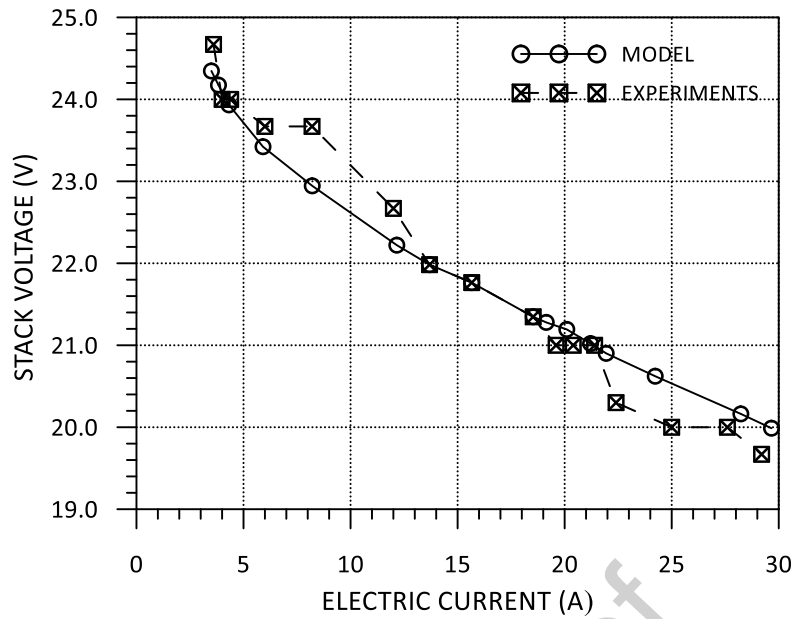
Figure 7. Polarisation curve of the PEMFC stack model

Figure 8 shows that higher PEMFC stack current is attained with decreasing external load resistance, as agreed by both model and experiments. The maximum discrepancy was 4.2%. Lower external load resistance means higher power demand from the PEMFC stack. Following the dependence of stack voltage with external current shown by Fig. 7, the increase of external load resistance increases the stack output voltage (Figure. 9). The maximum discrepancy between model and experiments for these results was 3.1%.
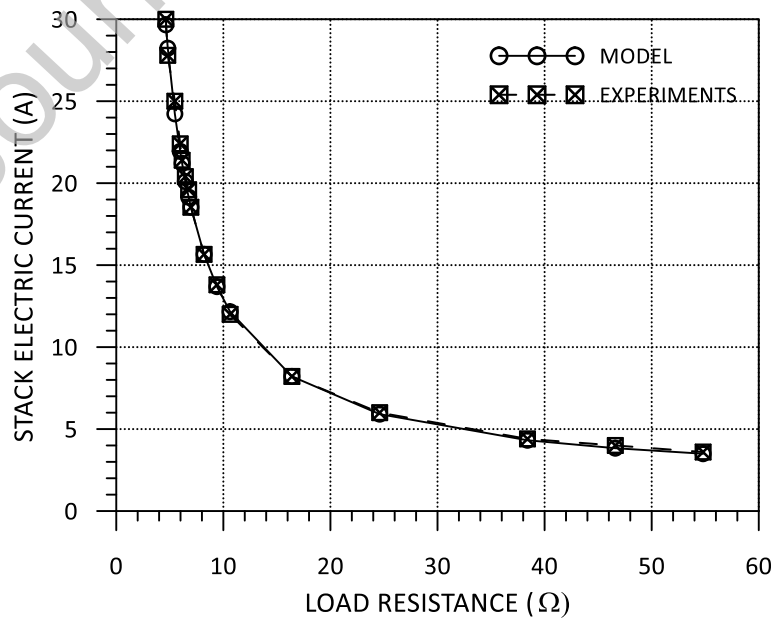

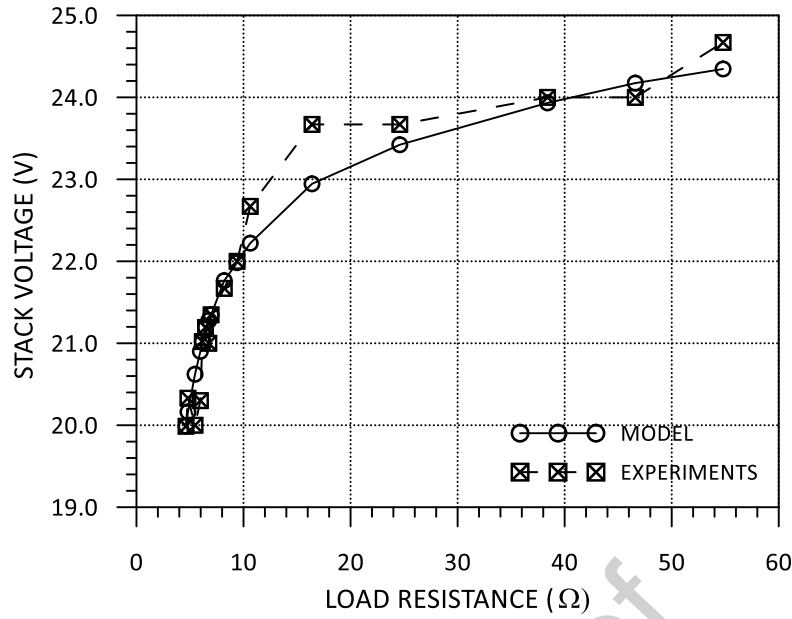Figure 8. Stack current variation with external load resistance

19

Figure 9. Stack voltage variation with external load resistance

In Figure it is noticed the increase of the stack output power with the decrease of the external load resistance. Model and experiments show similar trends, with a maximum discrepancy of 5.7%.
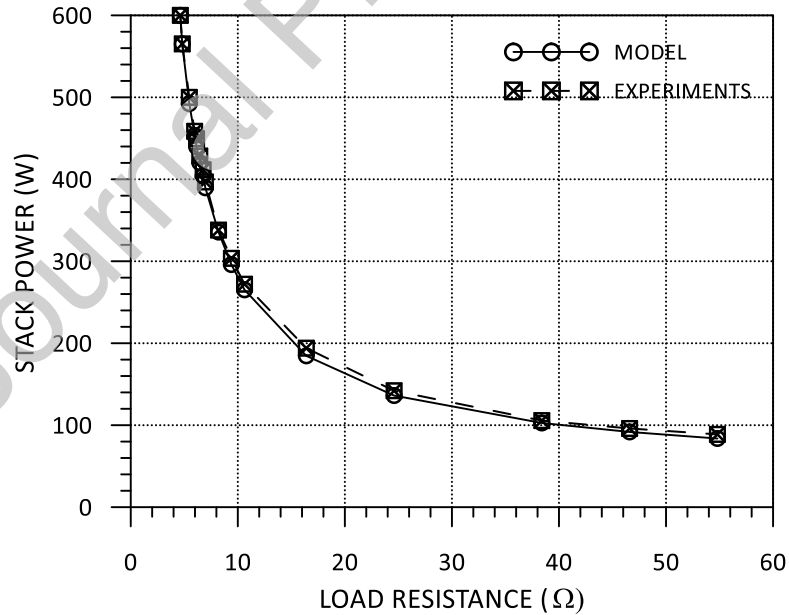

Figure 10. Output stack power variation with external load resistance

Fuel cell power output is incremental with the current (Figure 11) [50]; therefore, when a decrease in the external load resistance occurs, the stack raises its output current and, consequently, demands higher fuel flow rate (Figure 12). Both model and experiments show a

linear dependence of hydrogen consumption with stack current. The maximum discrepancy was 8.7%. When plotted against the output power, hydrogen flow rate also shows increasing values though the linearity is lost. A similar trend is reported by other authors [51]. Figure 13 shows hydrogen flow rate variation with output power.
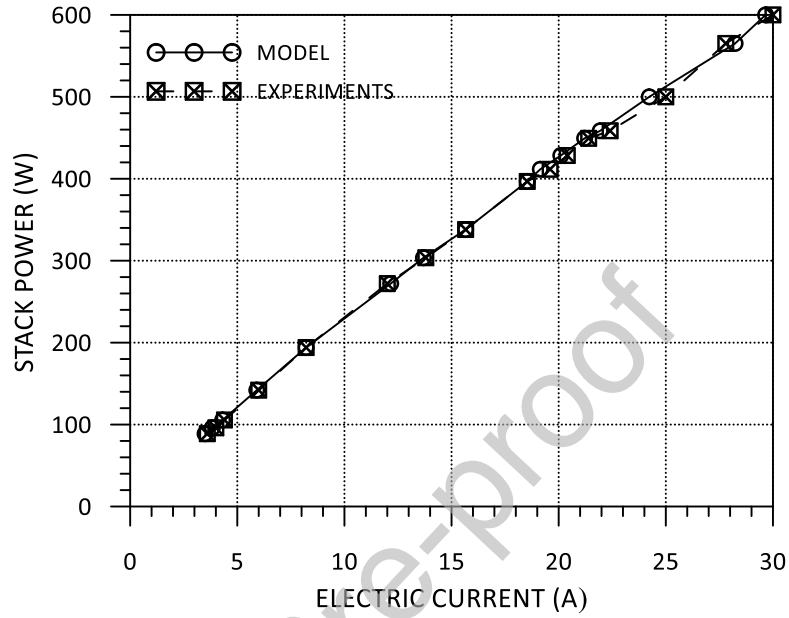
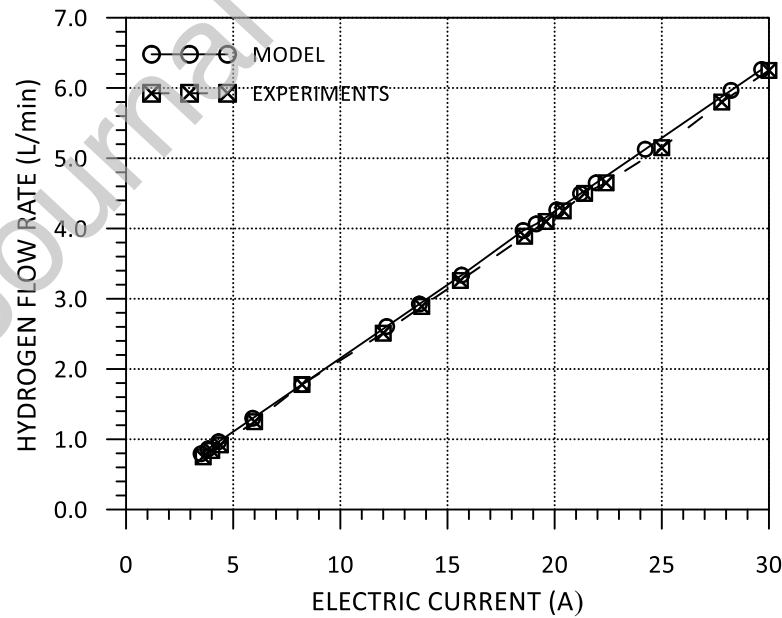Figure 11. Output stack power variation with electric current.

Figure 12. Hydrogen flow rate variation with electric current.
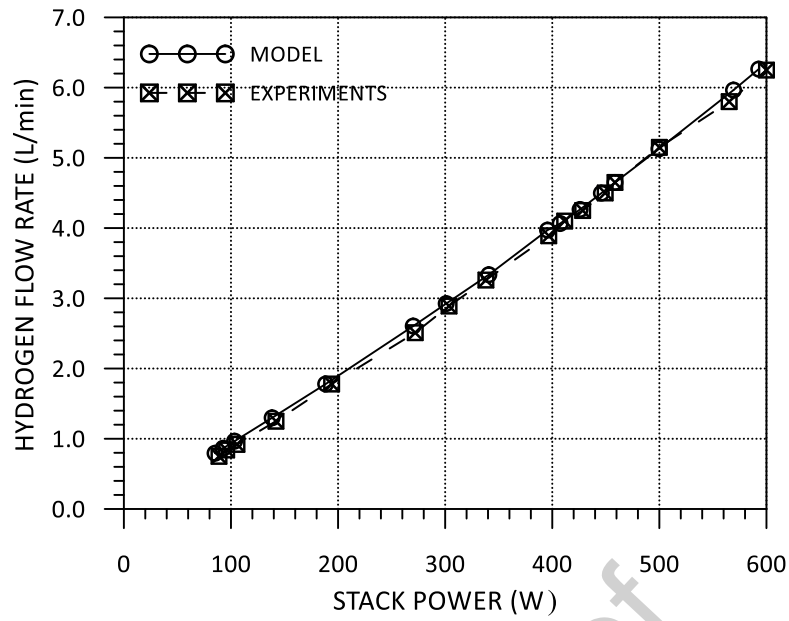
Figure 13. Hydrogen flow rate variation with output power.

Figure 14 shows the overall system efficiency predicted by the model and calculated from the experiments. The peak efficiencies were 47.6% (model) and 48.6% (experiments), attained at around 50% of the rated power. These values are below those reported by other authors, where peak efficiencies around 54% have been obtained [46, 51]. The maximum discrepancy was 4.6%. These results indicate there is a gap for fuel cell performance improvement, which is expected to be further explored in future works using the current model.

Figure 14. Variation of overall PEMFC system efficiency with output stack power

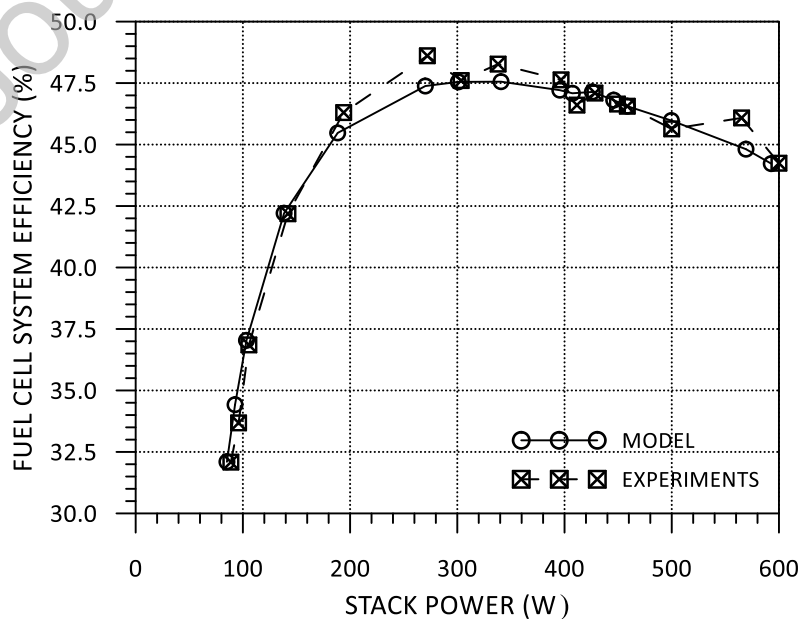The main advantages of using a simplified, one-dimensional fuel cell model such as the one here presented are the possibility to reduce development costs from experiments and, simultaneously, provide reasonably accurate results without long processing time. A previous study has shown that a one-dimensional model produced a close polarisation curve to a three-dimensional model, but with a processing period nearly 300 times faster [52]. The model here introduced can predict PEMFC performance from the assessment of various operating parameters, such as optimisation of stack temperature. With high operating temperature the fuel cell performance can be improved, but it will require more fan power that increases the operation cost.

5. CONCLUSION

A steady-state model that simulates a PEM fuel cell stack to calculate output power and overall system efficiency with varying external load was presented and compared with experiments in a test bench. In general, a good agreement between model and experiments was found for all results obtained. The stack polarisation curve, stack current and voltage variation with external load showed maximum discrepancies between model and experiments of 3.1%, 4.2% and 3.1%, respectively. The stack output power variation with load resistance presented a maximum discrepancy between model and experiments of 5.7%. Both model and experiments showed a linear dependence of hydrogen consumption with stack current, with a maximum discrepancy of 8.7%. Model and experiments revealed the maximum overall system efficiency of around 47.5% at 50% of the rated power. The maximum discrepancy of the system efficiency variation with output power determined by model and experiments was 4.6%. Future applications of the model include the investigation of operating parameters, such

23

as stack temperature, with aim to optimise the system for increased overall efficiency by decreasing fuel consumption and losses.

ACKNOWLEDGMENT

The authors thank the School of Engineering and Applied Science at Aston University and the University of Pisa for their support to this project.

REFERENCES

[1] F.N.Khatib, Tabbi Wilberforce, James Thompson, A.G.Olabi. Experimental and analytical study of open pore cellular foam material on the performance of proton exchange membrane electrolysers. International Journal of Thermofluids. Volume 9, February 2021, 100068. https://doi.org/10.1016/j.ijft.2021.100068.

[2] Wilberforce T, El-Hassan Z, Khatib FN, Al Makky A, Mooney J, Barouaji A, et al. Development of Bi-polar plate design of PEM fuel cell using CFD techniques. Int J Hydrogen Energy 2017. doi:10.1016/j.ijhydene.2017.08.093.

[3] Massimo Milani, Luca Montorsi, Gabriele Storchi, Matteo Venturelli, Diego Angeli, Adriano Leonforte, Davide Castagnetti, Andrea Sorrentino,. Experimental and numerical analysis of a liquid aluminium injector for an Al-H2O based hydrogen production system, International Journal of Thermofluids, Volumes 7–8, 2020, 100018, ISSN 2666-2027, https://doi.org/10.1016/j.ijft.2020.100018.

[4] Tabbi Wilberforce, O.Ijaodola, Emmanuel Ogungbemi, F.N.Khatib, T.Leslie, Zaki El-Hassan, J.Thomposon, A.G.Olabib. Technical evaluation of proton exchange membrane (PEM) fuel cell performance – A review of the effects of bipolar plates coating. Renewable and Sustainable Energy Reviews. Volume 113, October 2019, 109286. https://doi.org/10.1016/j.rser.2019.109286.

[5] Tabbi Wilberforce, O.Ijaodola, Emmanuel Ogungbemi, F.N.Khatib, Zaki El-Hassan, J.Thomposon, A.G.Olabi. A comprehensive study of the effect of bipolar plate (BP)

geometry design on the performance of proton exchange membrane (PEM) fuel cells. Renewable and Sustainable Energy Reviews. Volume 111, September 2019, Pages 236-260. https://doi.org/10.1016/j.rser.2019.04.081.

[6] Tabbi Wilberforce, O.Ijaodola, Emmanuel Ogungbemi, F.N.Khatib, Zaki El-Hassan, J.Thompson, A.G.Olabi. Numerical modelling and CFD simulation of a polymer electrolyte membrane (PEM) fuel cell flow channel using an open pore cellular foam material. Science of The Total Environment. Volume 678, 15 August 2019, Pages 728-740. https://doi.org/10.1016/j.scitotenv.2019.03.430.

[7] Ahmad Baroutaji, Tabbi Wilberforce, Mohamad Ramadan Abdul Ghani Olabi. Comprehensive investigation on hydrogen and fuel cell technology in the aviation and aerospace sectors. Renewable and Sustainable Energy Reviews. Volume 106, May 2019, Pages 31-40. https://doi.org/10.1016/j.rser.2019.02.022.

[8] O.S.Ijaodola, Zaki El- Hassan, E.Ogungbemi, F.N.Khatib, Tabbi Wilberforce, James Thompson, A.G.Olabi. Energy efficiency improvements by investigating the water flooding management on proton exchange membrane fuel cell (PEMFC). Energy. Volume 179, 15 July 2019, Pages 246-267.

[9] Tabbi Wilberforce, O.Ijaodola, Emmanuel Ogungbemi, F.N.Khatib, Zaki El-Hassan, J.Thompson, A.G.Olabi. Effect of humidification of reactive gases on the performance of a proton exchange membrane fuel cell. Science of The Total Environment. Volume 688, 20 October 2019, Pages 1016-1035. https://doi.org/10.1016/j.scitotenv.2019.06.397.

[10] Ijaodola O, Ogungbemi E, Khatib FN, Wilberforce T, Ramadan M, Hassan Z El, et al. Evaluating the Effect of Metal Bipolar Plate Coating on the Performance of Proton Exchange Membrane Fuel Cells. Energies 2018;11. doi:10.3390/en11113203.

[11] Tabbi Wilberforce, A. Alaswad, A. Palumbo, A. G. Olabi, Advances in stationary and portable fuel cell applications, International Journal of Hydrogen Energy 41(37) March 2016.

[12] Wilberforce T, Ijaodola O, Ogungbemi E, Hassan Z El, Thompson J, Olabi AG. Effect of

Bipolar Plate Materials on Performance of Fuel Cells. Ref. Modul. Mater. Sci. Mater. Eng., Elsevier; 2018. doi:10.1016/B978-0-12-803581-8.11272-X.

[13] Wilberforce T, Khatib FN, Ogungbemi E, Olabi AG. Water Electrolysis Technology. Ref. Modul. Mater. Sci. Mater. Eng., Elsevier; 2018. doi:10.1016/B978-0-12-803581-8.11273-1.

[14] Tabbi Wilberforce, Zaki El-Hassan, F.N.Khatib, Ahmed Al Makky, Ahmad Baroutaji, James G.Carton, Abdul G.Olabi. Developments of electric cars and fuel cell hydrogen electric cars. International Journal of Hydrogen Energy Volume 42, Issue 40, 5 October 2017, Pages 25695-25734. https://doi.org/10.1016/j.ijhydene.2017.07.054.

[15] T. Wilberforce, Z. El-Hassan, F.N. Khatib, A. Al Makyy, A. Baroutaji, J. G. Carton and A. G. Olabi, Modelling and Simulation of Proton Exchange Membrane Fuel cell with Serpentine bipolar plate using MATLAB, International journal of hydrogen, 2017. DOI: 10.1016/j.ijhydene.2017.06.091.

[16] Ogungbemi E, Ijaodola O, Khatib FN, Wilberforce T, El Hassan Z, Thompson J, et al. Fuel cell membranes – pros and cons. Energy 2019. doi:10.1016/J.ENERGY.2019.01.034.

[17] Tabbi Wilberforce, A. G. Olabi. Performance Prediction of Proton Exchange Membrane Fuel Cells (PEMFC) Using Adaptive Neuro Inference System (ANFIS). Sustainability 2020, 12, 4952; doi:10.3390/su12124952.

[18] Tabbi Wilberforce, A. G. Olabi. Design of Experiment (DOE) Analysis of 5-Cell Stack Fuel Cell Using Three Bipolar Plate Geometry Design. Sustainability 2020, 12, 4488; doi:10.3390/su12114488.

[19] A.G. Olabi, Tabbi Wilberforce, Enas Taha Sayed, Khaled Elsaid and Mohammad Ali Abdelkareem. Prospects of Fuel Cell Combined Heat and Power Systems. Energies 2020, 13(16), 4104; https://doi.org/10.3390/en13164104

[20] A.G.Olabi, Tabbi Wilberforce, Mohammad Ali Abdelkareem. Fuel cell application in the automotive industry and future perspective. Energy. Volume 214, 1 January 2021, 118955. https://doi.org/10.1016/j.energy.2020.118955.

[21] Mohammad Ali Abdelkareem, Tabbi Wilberforce, Khaled Elsaid, Enas Taha Sayed, Emad A.M.Abdelghani, A.G.Olabi. Transition metal carbides and nitrides as oxygen reduction reaction catalyst or catalyst support in proton exchange membrane fuel cells

(PEMFCs).International Journal of Hydrogen Energy. Available online 17 September 2020. https://doi.org/10.1016/j.ijhydene.2020.08.250

[22] Ogungbemi, E, Wilberforce, T, Ijaodola, O, Thompson, J, Olabi, AG. Review of operating condition, design parameters and material properties for proton exchange membrane fuel cells. *Int J Energy Res*. 2020; 1– 19. https://doi.org/10.1002/er.5810

[23] Mohammed Ali Abdelkareem, Khaled Elsaid, Tabbi Wilberforce, Mohammed Kamil, Enas Taha Sayed, A.Olabi. Environmental Aspect of Fuel cell – A review. Science of The Total Environment. Volume 752, 15 January 2021, 141803. https://doi.org/10.1016/j.scitotenv.2020.141803.

[24] Emmanuel Ogungbemi, Tabbi Wilberforce, Oluwatosin Ijaodola, James Thompson, A.G.Olabi. Selection of proton exchange membrane fuel cell for transportation. International Journal of Hydrogen Energy. Available online 28 July 2020. https://doi.org/10.1016/j.ijhydene.2020.06.147

[25] Ahmad Baroutaji, Arun Arjunan, Abed Alaswad, Ayyappan S.Praveen, Tabbi Wilberforce, Mohammad A.Abdelkareem, Abdul-Ghani Olabi. Materials for Fuel Cell Membranes. Reference Module in Materials Science and Materials Engineering. 2020. https://doi.org/10.1016/B978-0-12-815732-9.00034-6.

[26] A.Al-Anazi, Tabbi Wilberforce, F.N.Khatib, P.Vichare, A.G.Olabi. Performance evaluation of an air breathing polymer electrolyte membrane (PEM) fuel cell in harsh environments – A case study under Saudi Arabia's ambient condition. International Journal of Hydrogen Energy. https://doi.org/10.1016/j.ijhydene.2020.10.258.

[27] Enas Taha Sayed, Mohammad Ali Abdelkareem, Mohamed S. Mahmoud, Ahmad Baroutaji, Khaled Elsaid, Tabbi Wilberforce, Hussein M. Maghrabie, G. Olabi, Augmenting Performance of Fuel Cells Using Nanofluids, Thermal Science and Engineering Progress, 2021, 101012, ISSN 2451-9049, https://doi.org/10.1016/j.tsep.2021.101012.

[28] Ahmad Baroutaji, Arun Arjunan, Mohamad Ramadan, John Robinson, Abed Alaswad, Mohammad Ali Abdelkareeme, Abdul-Ghani Olabi. Advancements and prospects of thermal management and waste heat recovery of PEMFC. International Journal of Thermofluids. Volume 9, February 2021, 100064. https://doi.org/10.1016/j.ijft.2021.100064.

[29] Baschuk JJ, Li X. Mathematical model of a PEM fuel cell incorporating CO poisoning

and O$_2$ (air) bleeding. Int J Glob Energy Issues 2003;20:245. https://doi.org/10.1504/IJGEI.2003.003966.

[30] Cheng S, Fang C, Xu L, Li J, Ouyang M. Model-based temperature regulation of a PEM fuel cell system on a city bus. Int J Hydrogen Energy 2015;40:13566–75. https://doi.org/10.1016/j.ijhydene.2015.08.042.

[31] Mokrani Z, Rekioua D, Mebarki N, Rekioua T, Bacha S. Proposed energy management strategy in electric vehicle for recovering power excess produced by fuel cells. Int J Hydrogen Energy 2017;42:19556–75. https://doi.org/10.1016/j.ijhydene.2017.06.106.

[32] Muñoz PM, Correa G, Gaudiano ME, Fernández D. Energy management control design for fuel cell hybrid electric vehicles using neural networks. Int J Hydrogen Energy 2017;42:28932–44. https://doi.org/10.1016/j.ijhydene.2017.09.169.

[33] Amiri A, Vijay P, Tadé MO, Ahmed K, Ingram GD, Pareek V, Utikar R. Planar SOFC system modelling and simulation including a 3D stack module. Int J Hydrogen Energy 2016;41:2919–30. https://doi.org/10.1016/j.ijhydene.2015.12.076.

[34] Tang S, Amiri A, Tadé MO. System level exergy assessment of strategies deployed for solid oxide fuel cell stack temperature regulation and thermal gradient reduction. Ind Eng Chem Res 2019;58:2258-67. https://doi.org/10.1021/acs.iecr.8b04142.

[35] Benziger JB, Satterfield MB, Hogarth WHJ, Nehlsen JP, Kevrekidis IG. The power performance curve for engineering analysis of fuel cells. J Power Sources 2006;155:272–285. https://doi.org/10.1016/j.jpowsour.2005.05.049.

[36] Barbir F. PEM fuel cells : theory and practice. 2nd Ed. USA: Academic Press; 2013. https://doi.org/10.1016/B978-0-12-387710-9.01001-8.

[37] Hooper MAI, Mann RF, Roberge PR, Amphlett JC, Jensen HM, Peppley BA. Development and application of a generalised steady-state electrochemical model for a PEM fuel cell. J Power Sources 2002;86:173–80. https://doi.org/10.1016/s0378-

7753(99)00484-x.

[38] Pathapati PR, Xue X, Tang J. A new dynamic model for predicting transient phenomena in a PEM fuel cell system. Renew Energy 2005;30:1–22. https://doi.org/10.1016/j.renene.2004.05.001.

[39] O'Hayre R, Cha S, Colella W, Prinz F. Fuel cell fundamentals. 3rd Ed. New Jersey: John Wiley & Sons, Inc; 2009. https://doi.org/10.1007/978-0-387-73532-0_1.

[40] Saleh IMM, Ali R, Zhang H. Simplified mathematical model of proton exchange membrane fuel cell based on horizon fuel cell stack. J Mod Power Syst Clean Energy 2016;4:668–79. https://doi.org/10.1007/s40565-016-0196-5.

[41] Leon Yu T-L, Lin H-L. Preparation of PBI/H 3 PO 4 -PTFE composite membranes for high temperature fuel cells. The Open Fuels & Energy Sci J 2010;3:1-7. https://doi.org/10.2174/1876973X01003010001

[42] Andújar JM, Segura F, Vasallo MJ. A suitable model plant for control of the set fuel cell−DC/DC converter. Renew Energy 2008;33:813–26. https://doi.org/10.1016/j.renene.2007.04.013.

[43] Rogers E. Understanding boost power stages in switchmode power supplies. Texas Instrument Application Report; 1999 March. Report No.: SLVA061.

[44] Pavlovic T, Bjazic T, Ban Z. Modeling and current control of fuel cell-battery hybrid system with boost converter and input-output filters. 15th International Power Electronics and Motion Control Conference (EPE-PEMC); 2012 Sep 4-6; Novi Sad, Serbia. IEEE; 2013. https://doi.org/10.1109/EPEPEMC.2012.6397212.

[45] Gauchía L, Martínez JM, Chinchilla M, Sanz J. Test bench for the simulation of a hybrid power train. 2007 European Conference on Power Electronics and Applications; 2007 Sep 2-5; Aalborg, Denmark. IEEE; 2008. https://doi.org/10.1109/EPE.2007.4417235.

[46] Yun H, Zhao Y, Wang J. Modeling and simulation of fuel cell hybrid vehicles. Int J Automotive Technol 2010;11:223-8. https://doi.org/10.1007/s12239−010−0028−y

[47] Mahjoubi C, Olivier J-C, Skander-Mustapha S, Machmoum M, Slama-Belkhodja I. An improved thermal control of open cathode proton exchange membrane fuel cell. Int J Hydrogen Energy 2019;44:11332–45. https://doi.org/10.1016/j.ijhydene.2018.11.055.

[48] Marignetti F, Minutillo M, Perna A, Jannelli E. Assessment of fuel cell performance under different air stoichiometries and fuel composition. IEEE Trans Ind Electron 2011;58:2420-6. https://doi.org/10.1109/TIE.2010.2069073

[49] Hua Z, Xua L, Lia J, Gana Q, Xub X, Ouyanga M, Songa Z, Kim J. A multipoint voltage-monitoring method for fuel cell inconsistency analysis. Energy Convers Manag 2018;177:572–81 https://doi.org/10.1016/j.enconman.2018.09.077.

[50] Prabha Acharya, Prasad Enjeti, Ira J. Pitel. An Advanced Fuel Cell Simulator. APEC '04 - Nineteenth Annual IEEE Applied Power Electronics Conference and Exposition; 2004 Feb 22-26; Anaheim, USA. IEEE; 2004. https://doi.org/ 10.1109/APEC.2004.1296071.

[50] Jin Z, Ouyang M, Lu Q, Gao D. Development of fuel cell hybrid powertrain research platform based on dynamic testbed. Int J Automotive Technol 2008;9:365-72. https://doi.org/10.1007/s12239−008−0044−3

[51] Falcão DS, Gomes PJ, Oliveira VB, Pinho C, Pinto AMFR. 1D and 3D numerical simulations in PEM fuel cells. Int J Hydrogen Energy 2011;36:12486–98. https://doi.org/10.1016/j.ijhydene.2011.06.133.

Declaration of interests

☒ The authors declare that they have no known competing financial interests or personal relationships that could have appeared to influence the work reported in this paper.

☐The authors declare the following financial interests/personal relationships which may be considered as potential competing interests: